Evaluating Accumulation of Fatigue Damage in Steel Bridges Using Measured Strain Data

JEREMIAH FASL, TODD HELWIG, SHARON L. WOOD, and KARL FRANK

ABSTRACT

As traffic volumes increase, bridges age, and maintenance budgets are cut, transportation officials often need quantitative data to distinguish between bridges that can be kept safely in service and those that need to be replaced or retrofitted. Strain gages can be utilized to evaluate fatigue damage in steel bridges using the techniques that are discussed in this paper. To evaluate fatigue damage, the cycles induced by vehicular traffic must be quantified using a cycle-counting algorithm, such as a rainflow algorithm. The amount of fatigue damage induced during the monitoring period can then be calculated using the traditional method, the effective stress range, or using a new approach based on the index stress range. One distinct advantage of the proposed method is that the relative amount of fatigue damage accumulated at different locations along the bridge can be easily compared. The advantages and limitations of both methods are demonstrated using measured data from a fracture-critical steel bridge.

Keywords: strain gages, fatigue measurement, steel bridges.

INTRODUCTION

Transportation officials face the difficult task of maintaining the nation's inventory of highway bridges under the pressure of reduced maintenance budgets, aging infrastructure, and increasing traffic volumes. One of the critical types of structural deterioration for steel bridges is fatigue-induced fracture. The primary method used to identify structural deterioration is hands-on visual inspections, the results of which provide transportation officials with qualitative data relative to the location and growth of cracks. However, quantitative data are often needed to distinguish between bridges that can safely remain in service and bridges that need to be replaced or retrofitted. Using the measured strain response of the bridge under service loads to evaluate the accumulation of fatigue damage is one means of providing this quantitative data.

Techniques for evaluating the accumulation of fatigue damage from measured strain data are discussed in this paper. In all cases, rainflow analyses are used to determine the spectrum of stresses at the location of each strain gage. Potential drawbacks of using the effective stress range, which is the traditional technique used for tracking fatigue damage, are presented. The index stress range is introduced as a means of easily determining the relative accumulation of fatigue damage at multiple locations along a bridge. Techniques for visualizing fatigue damage accumulation are also presented. The measured response of a fracture-critical steel bridge is used to demonstrate the methods discussed in this paper.

Jeremiah Fasl, Associate III, Wiss, Janney, Elstner Associates Inc., Austin, TX (corresponding). Email: jfasl@wje.com

Todd Helwig, Associate Professor, University of Texas–Austin. Email: thelwig@mail.utexas.edu

Sharon L. Wood, Interim Dean, Cockrell School of Engineering, University of Texas–Austin. Email: swood@utexas.edu

Karl Frank, Chief Engineer, Hirschfeld Industries. Email: karl.frank@hirschfeld.com

Paper No. 2013-27

BACKGROUND

Before 1970, the fatigue guidelines in the AASHTO bridge design specifications were based on the measured response of small-scale specimens that were tested under constant-amplitude loading (Schilling et al., 1978). These tests revealed that the primary variables affecting fatigue life were the stress range and configuration of the connection detail (Schilling et al., 1978). In addition, a stress range was identified, the constant-amplitude fatigue limit, S_{th}, below which the fatigue life was expected to be infinite. These concepts serve as the basis for the S-N curves (Figure 1) used in the current bridge design specifications in the United States (AASHTO, 2010).

According to the AASHTO Load and Resistance Bridge Design (LRFD) Specifications (2010), for a given constant-amplitude stress range, S_r, that exceeds the constant-amplitude fatigue limit, the number of cycles to failure, N_f, can be calculated using Equation 1:

$$N_f = \frac{A}{S_r^3} \tag{1}$$

where A is the fatigue constant for the detail category defined by AASHTO (2010). Equation 1 is used for the design of new bridges; therefore, the fatigue constant for each detail category corresponds to a low probability of failure.

Although fatigue tests have traditionally been conducted using a constant-amplitude stress range, highway bridges are subjected to stress cycles with varying amplitudes under service loads. A cumulative damage theory is used to calculate the effective stress range for a given spectrum of variable-amplitude stress cycles. The most common damage theory is Palmgren-Miner's rule (ASCE, 1982), which is based on a linear damage hypothesis. The Palmgren-Miner rule for linear damage accumulation is simple to use, and the results agree with experimental data (ASCE, 1982). Nonlinear cumulative damage theories have been proposed (i.e., Li, Chan and Ko, 2001); however, the equations are more complicated to use and the results are not consistently better than a linear damage model (ASCE, 1982).

For a connection detail subjected to constant-amplitude stress cycles, the accumulated damage ratio, D, represents the portion of the design life that has been consumed by the imposed loading cycles:

$$D = \frac{n}{N_f} \tag{2}$$

where n is the number of imposed loading cycles. For a variable-amplitude stress spectrum, the accumulated damage ratio is the sum of the fatigue damage induced by each stress range within the spectrum:

$$D = \sum_{j=1}^{k} \frac{n_j}{N_{fj}} \tag{3}$$

where n_j is the number of cycles imposed with a stress range of S_{rj}, N_{fj} is the number of cycles corresponding to failure at a stress range of S_{rj} and k is the number of distinct stress ranges included within the stress spectrum. If Equation 1 is substituted into Equation 3, the damage accumulation ratio can be expressed in terms of the number of cycles imposed in each stress range, n_j, and the cube of the individual stress ranges, S_{rj}:

$$D = \sum_{j=1}^{k} \frac{n_j \times S_{rj}^3}{A} \tag{4}$$

Note that the damage accumulation ratio is tied to the design value of the fatigue life, rather than to the median fatigue life, for a given connection detail.

As indicated in Figure 1, the design *S-N* relationships are typically shown as log-log plots. If the damage accumulation ratio is included in the same graph, lines corresponding to constant values of D are parallel to the descending branch of the *S-N* relationship (Figure 2). Therefore, the damage accumulation ratio can be considered the portion of the design fatigue life that has been consumed during the monitoring period of the bridge.

In the previous discussion, it was assumed that the components of the stress spectrum were known. However, when using measured strain data to evaluate the fatigue response of a bridge, a cycle-counting algorithm must be used to transform the strain history into a stress spectrum, which is expressed in terms of a histogram of stress amplitudes. The simplified rainflow method outlined by Downing and Socie (1982) and included in ASTM E1049 (2011) was used for all analyses discussed in this paper. The method is well suited for fatigue analysis because it counts cycles based on closed hysteresis loops (Dowling, 1972).

Schilling and colleagues (1978) introduced the concept of an effective stress range for characterizing the fatigue resistance of connection details subjected to variable-amplitude loading. The fatigue damage induced by a spectrum of stress cycles is the same as the fatigue damage induced by the total number of stress cycles within the spectrum, n_m, at the effective stress range, S_{re}:

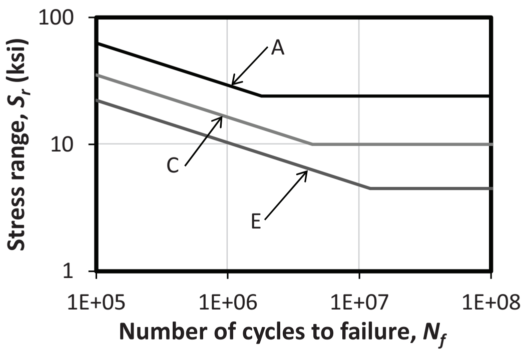

Fig. 1. Representative S-N *design relationships from AASHTO (2010).*

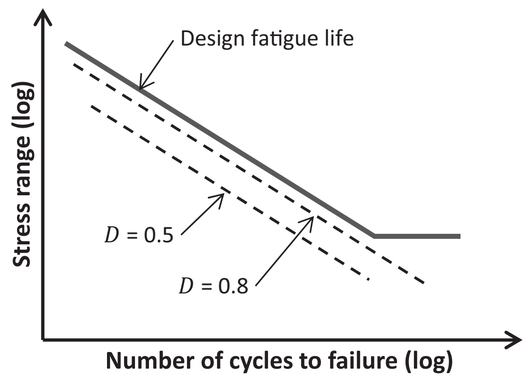

Fig. 2. Different levels of the damage accumulation ratio superimposed on S-N *relationship used for design.*

$$D = \frac{n_m \times S_{re}^3}{A} \tag{5}$$

Setting Equation 5 equal to Equation 4 leads to the definition of the effective stress range:

$$S_{re} = \left(\sum_{j=1}^{k} \frac{n_j}{n_m} S_{rj}^3 \right)^{1/3} \tag{6}$$

The relationship between the total number of stress cycles, n_m, the effective stress range, S_{re}, and the damage accumulation ratio, D, is illustrated in Figure 3. The total number of stress cycles within the stress spectrum is calculated using the rainflow counting algorithm to evaluate the measured strain history. The damage accumulation ratio is calculated from the stress spectrum using Equation 5. The effective stress range can also be calculated from the stress spectrum using Equation 6.

The effective stress range is an efficient method to relate the cycles from a spectrum of stress ranges to a single, equivalent stress range. The single, equivalent stress range is a useful metric because it can be used to calculate the remaining fatigue life, as discussed in Fasl (2013). One of the limitations of this traditional approach for evaluating the accumulation of fatigue damage from measured strain data is that both the effective stress range and the total number of cycles during the monitoring period must be used to characterize the extent of fatigue damage at a given location. Nonetheless, both of these parameters vary with location along the bridge, which complicates comparison of fatigue data from multiple sensors using the effective stress range as the sole parameter.

To illustrate that limitation, the effective stress range and number of cycles for three representative gage locations are presented (Figure 4). Because both the effective stress range and number of cycles are larger for gage b than for gage a, it is obvious that gage b has a higher accumulation of damage than gage a. Likewise, because the number of cycles for gage c is larger than gage a, while the effective stress ranges are equal, gage c has a higher accumulation of damage than gage a. Nonetheless, comparing the relative accumulation of damage between gages b and c is more complicated. Gage b has a higher effective stress range but a fewer number of cycles than gage c. Using the historical method of evaluating fatigue, the only way to compare the two gage locations would be to calculate the remaining fatigue life or plot the damage accumulation ratio (Figure 4). A new approach, the index stress range, which is introduced later in this paper, was developed to quantify the relative accumulation of damage between gages.

Data from a fracture-critical steel bridge that was monitored for nearly a year by the research team were used in this paper to highlight the advantages of using the index stress range to evaluate the accumulation of fatigue data.

DESCRIPTION OF BRIDGE

The strain response of a fracture-critical steel bridge with significant truck traffic was monitored as part of this investigation. The average daily truck traffic was reported as 4,000 trucks per day, with nearly 60 percent of those trucks featuring five or more axles. The bridge was constructed in 1935 and comprises three spans (73.5-ft end spans and a 125-ft center span) for a total length of 272 ft (Figure 5). The longitudinal girders in the end spans are continuous over the interior supports and extend 30.5 ft into the center span. The bridge is statically determinate, and the center section is suspended by hangers between the overhangs within the middle span. The bridge is considered to be fracture critical

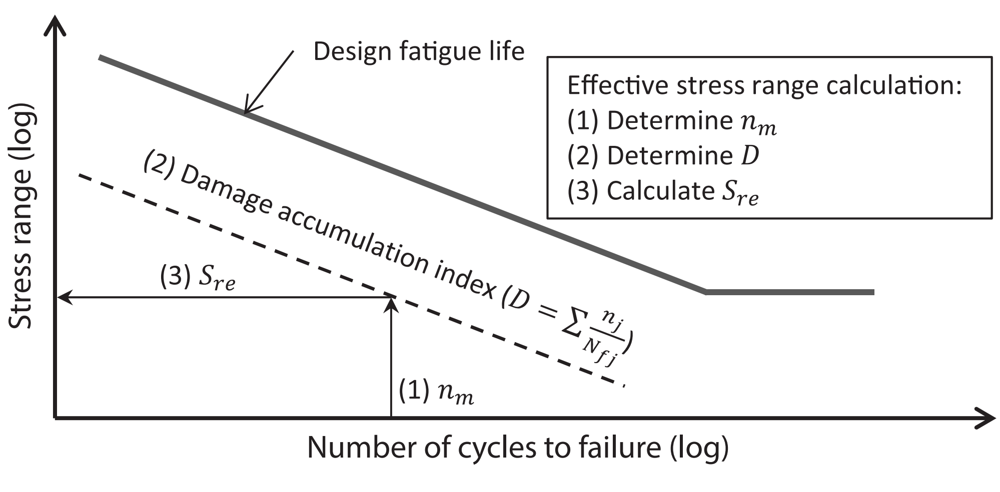

Fig. 3. Graphical representation of the method used to determine the effective stress range for a given stress spectrum.

because the superstructure includes only two longitudinal girders and the failure of a flange from one girder would be expected to lead to the collapse of the entire bridge.

The longitudinal girders are built-up sections (Figure 6) that are spaced 23 ft apart (center-to-center). The girders are haunched, with a girder depth of 8 ft over the interior piers, 5 ft at midspan of the bridge and 5.54 ft at the end supports. Double angles serve as the flanges of the built-up section and were riveted to the web plate. Cover plates were riveted to the flanges near the interior supports and at the center of the suspended span to increase the moment capacity. Transverse floor beams provide lateral support for the longitudinal girders and are spaced 7.5 ft on-center along the length of the bridge. The webs of the floor beams are riveted to angles that serve as stiffeners for the longitudinal girders. Traffic originally traveled in both the southbound and northbound directions.

In 1974, the deck of the bridge was widened and welds were added to connect the top flange of the longitudinal girders to the top flange of the floor beams and to the top flange of the brackets that support the overhang (Figure 6). A plan view of the detail is presented in Figure 7. The widened deck was not made composite with the longitudinal girders. When the bridge was widened, a separate bridge was added for southbound traffic; therefore, traffic currently crosses the bridge in the northbound direction of the two-lane steel bridge. Accordingly, over the entire life of the bridge, the majority of the trucks are expected to cross the bridge in the right lane, which is supported by the east girder.

The welds that were added for the bridge widening correspond to a category E detail (AASHTO, 2010). Reports from recent inspections conducted by the bridge owner indicated that cracks had formed and were growing at the welded connections between the longitudinal girders and floor beams at locations where the cover plates were not present (Figure 8). Although the live load moments were calculated to

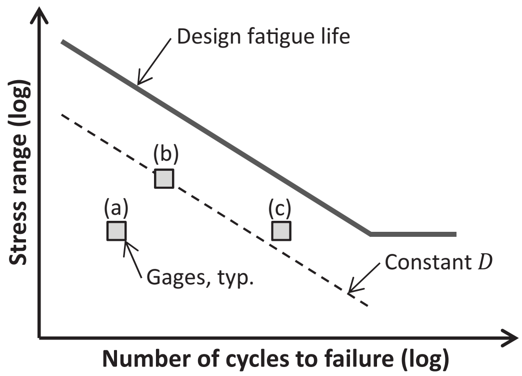

Fig. 4. Comparison of relative damage levels for three gage locations.

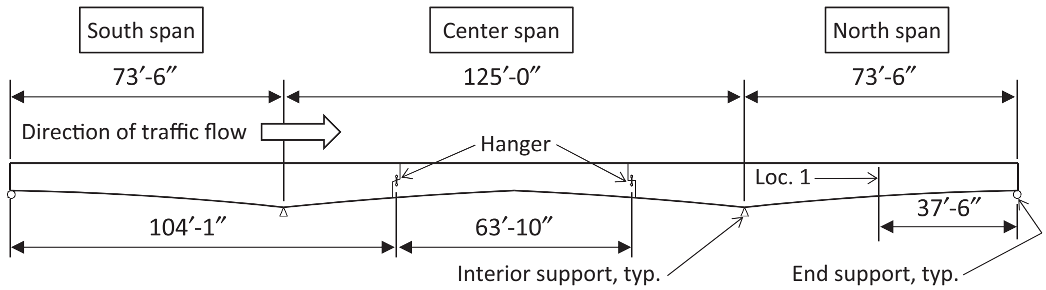

Fig. 5. Elevation of the bridge and location of strain gages.

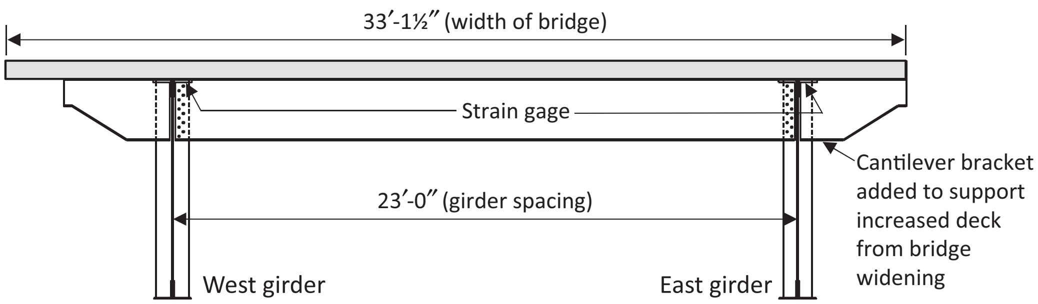

Fig. 6. Cross-section of the bridge (looking north).

be greater at the interior supports, the flexural stresses in the longitudinal girders were calculated to be greater at the locations of the observed cracks because the moment of inertia was less.

Strain gages were installed on both the top and bottom flanges of the longitudinal girders at several locations along the length of the bridge. The complete set of strain data is presented in Fasl (2013). In this paper, only data collected from strain gages installed on the top flange of each longitudinal girder (Figure 6) at location 1 near the north support (Figure 5) are presented. To monitor the live load response of the longitudinal girder, the strain gages were installed 2 ft south of the connection between the stiffener angles and the floor beams/brackets.

At the location of the strain gages, negative moment is induced when a vehicle is in the center span and positive moment is induced when a vehicle is in the north span. The difference in strain readings between the maximum positive and maximum negative readings determines the maximum stress range for a given vehicle crossing the bridge.

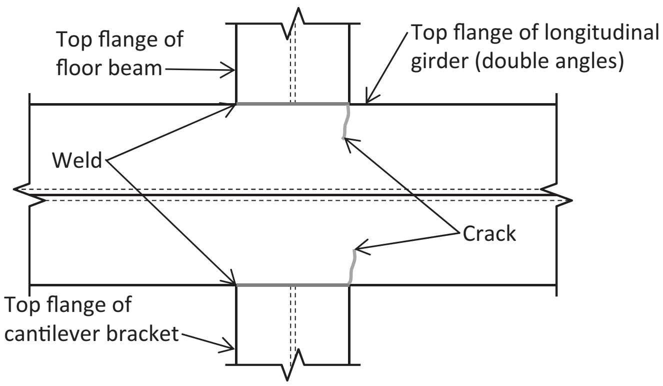

Fig. 7. Plan view of category E detail.

MEASURED RESPONSE OF BRIDGE

The research team collected strain data for 71 days at an effective scan rate of 50 Hz. Strain histories were analyzed in 30-min segments to minimize the errors associated with temperature drift (Fasl et al., 2010). A minimum cycle amplitude of 2 microstrain (0.06 ksi) was used when processing the data to avoid counting cycles attributed to electromechanical noise within the data acquisition system. Strains were converted to stresses using Hooke's law and a modulus of elasticity for steel of 29,000 ksi.

The resulting histograms corresponding to the stress spectra are shown in Figure 9. Two hundred bins were used in the rainflow analyses; each bin was 5 microstrain (0.15 ksi) wide. The data are presented in terms of the average number of cycles per day to facilitate comparisons with other bridges. Each gage experienced several extremely large-amplitude stress cycles (>15 ksi) during the 71-day monitoring period.

The bridge was expected to have a finite fatigue life because a large portion of the cycles in the stress spectra for each girder exceeded the constant amplitude fatigue limit for category E details (4.5 ksi). This assumption was confirmed by the rate of crack growth observed at several of the welded connections (Fasl, 2013).

For this bridge, evaluation of the accumulated fatigue damage at the locations of the two strain gages was straightforward. The stress spectrum for the east girder included an average of 56,000 cycles/day with an effective stress range of 2.26 ksi. In contrast, the stress spectrum for the west girder included an average of 38,000 cycles/day with an effective stress range of 1.44 ksi. Because both the effective stress range and the number of cycles were greater for the east girder, the east girder accumulated more fatigue damage than the west girder during the monitoring period. This observation was expected because traffic currently crosses the bridge only in the northbound direction and the east girder is below the right lane of traffic; therefore, the

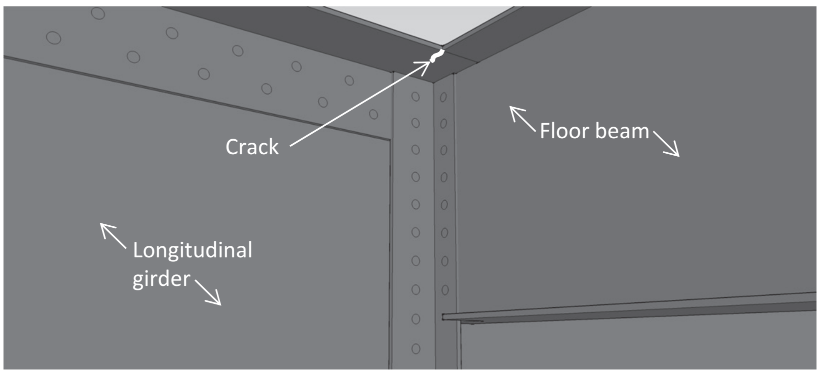

Fig. 8. Three-dimensional schematic of crack at weld between the floor beam and longitudinal girder.

volume of truck traffic is expected to be higher in the right lane rather than the left lane. However, the relative accumulation rates of fatigue damage in the two girders are not readily apparent from the results of this analysis.

INDEX STRESS RANGE

The index stress range method was proposed by Fasl and colleagues (2012) as a means of expressing the fatigue damage accumulation in terms of a single parameter. This method facilitates comparisons among multiple strain gages positioned along the same bridge and can also be used to compare the accumulation rate of fatigue damage among bridges within an inventory of bridges.

The method is summarized in Figure 10. As a first step, the engineer selects the value of the index stress range, $\hat{S}_{ri}$, to be used in the calculations. Although the choice is arbitrary, the constant-amplitude fatigue limit, S_{th}, is a convenient choice. Then the effective number of cycles at the index stress range, $\hat{n}_i$, is calculated such that the accumulated fatigue damage induced is the same as that induced by the measured stress spectrum:

$$D = \sum_{j=1}^{k} \frac{n_j \times S_{rj}^3}{A} = \frac{\hat{n}_i \times \hat{S}_{ri}^3}{A} \tag{7}$$

The effective number of cycles at the index stress range can be calculated by rearranging the terms in Equation 7:

$$\hat{n}_i\left(\hat{S}_{ri}\right) = \sum_{j=1}^{k} \frac{n_j \times S_{rj}^3}{\hat{S}_{ri}^3} \tag{8}$$

For the stress spectra shown in Figure 9, and an index stress range equal to S_{th} [4.5 ksi for category E details (AASHTO, 2010)], the east girder experienced an average of 7,100 equivalent stress cycles a day compared with an average of 1,250 equivalent stress cycles a day for the west girder. The advantage of the method is that the relative amount of damage can be determined directly because the data are normalized to the same stress range. For instance,

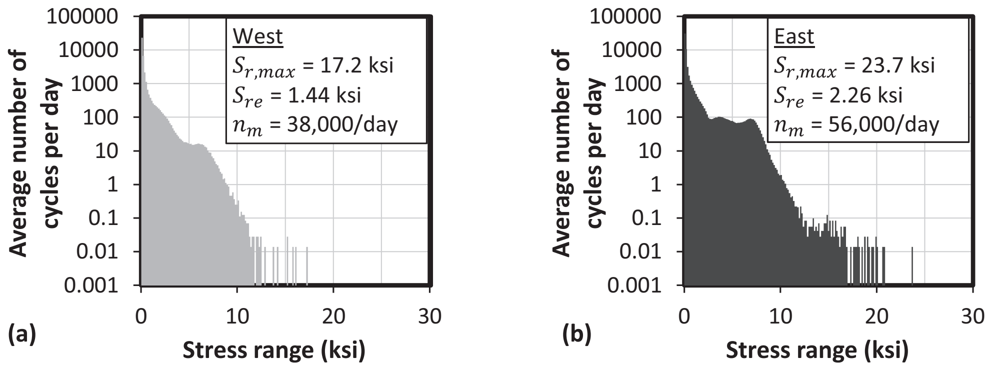

Fig. 9. Stress spectra calculated from the strain histories recorded from the top flange of the (a) west girder and (b) east girder.

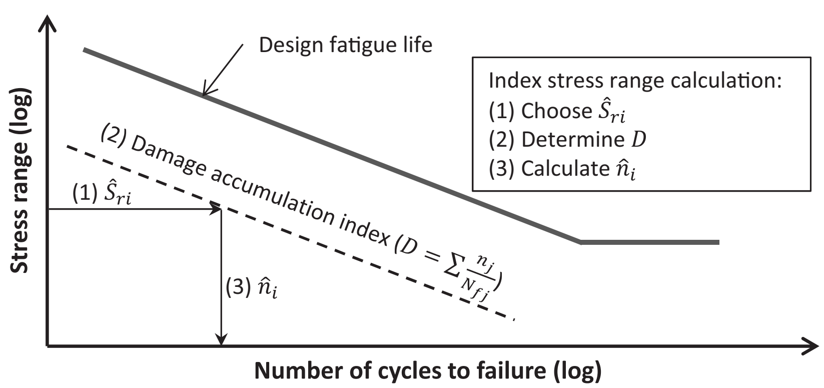

Fig. 10. Graphical representation of the method used to determine the effective number of cycles at the index stress range for a given stress spectrum.

at this bridge, the east girder accumulated 5.5 (7,100/1,250) times as much damage as the west girder during the monitoring period.

If a different value had been selected for the index stress range, the number of equivalent stress cycles would be different, but the fatigue damage accumulation ratio for each girder would remain unchanged. Therefore, direct comparisons of the relative amount of fatigue damage are always possible.

VISUALIZATION OF FATIGUE DAMAGE

The advantages of the index stress method extend beyond the direct means of comparing the accumulation of fatigue damage from different stress spectra. The index stress method also provides a means of visualizing the impact of decisions made during the processing of raw strain data.

One concern associated with using the Palmgren-Miner rule with stress spectra corresponding to measured strain data is the influence of low-amplitude stress cycles (Fisher, Kulak and Smith, 1998). When tested in the laboratory using constant-amplitude stress cycles, connection details exhibited an infinite fatigue life when the amplitude of the applied stress cycles was less than S_{th}. However, for variable-amplitude fatigue, there is not agreement on the influence of cycles with stress ranges below S_{th}. Swenson and Frank (1984) showed that all cycles contribute to the accumulation of fatigue damage, while Connor and Fisher (2006) recommended truncating cycles with amplitudes less than 25 to 50% of S_{th} from the measured stress spectrum.

Despite the lack of consensus, many engineers truncate data without analyzing the impact of all cycles on the accumulation of fatigue damage. As such, new visualization techniques were developed and are discussed herein to allow an engineer to assess the influence of all stress ranges to the accumulation of fatigue damage.

If traditional approaches are used to characterize the accumulated fatigue damage, both the effective stress range and the number of cycles vary as the lower amplitude cycles are truncated from the stress spectrum. Data from the east longitudinal girder are plotted in Figure 11. The horizontal axis corresponds to the ratio of the minimum stress range retained in the stress spectrum, $S_{r,\min}$, to the constant-amplitude fatigue limit, S_{th}.

Because a large number of low-amplitude cycles are included in the stress spectrum (Figure 9b), the number of cycles included in the calculations decreased rapidly as the lower-amplitude cycles were truncated from the spectrum. If all cycles less than $0.1S_{th}$ were truncated, the total number of cycles within the stress spectrum decreased by more than 80%. In contrast, the effective stress range increased by more than 100% if all cycles less than $0.2S_{th}$ were truncated. These changes in n_m and S_{re} imply that the accumulated fatigue damage is extremely sensitive to the value of $S_{r,\min}$ used in the calculations. However, the damage accumulation ratio, D, decreased by less than 5% when $S_{r,\min}$ was taken as $0.5S_{th}$. This example highlights the interactions between S_{re} and n_m and demonstrates that using only the effective stress range to characterize the accumulated fatigue damage is misleading.

In contrast, the effective number of cycles at the index stress level, $\hat{n}_i$, provides a clear interpretation of the relationship between the accumulated fatigue damage and $S_{r,\min}$ (Figure 12). In this case, a single parameter is sufficient to characterize the accumulation of fatigue damage.

The previous discussion focused on the influence of low-amplitude stress cycles on the accumulation of fatigue damage. The techniques discussed in this paper can also be used to identify the stress ranges within a measured spectrum that have the largest influence on the fatigue damage accumulation. When utilizing stress spectra acquired in the field, engineers are typically concerned whether the lower and higher stress ranges are load induced or are due to limitations of the data acquisition system. Electromechanical noise in the data acquisition equipment can cause fictitious low-amplitude cycles, whereas lightning strikes or CB

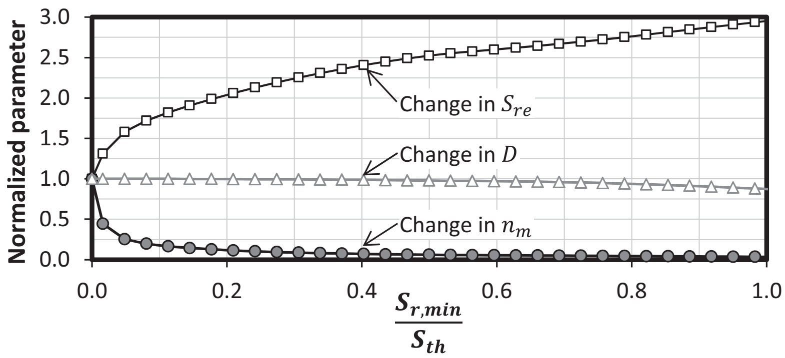

Fig. 11. Sensitivity of effective stress range and number of cycles to the minimum stress range retained in the stress spectrum for the east girder.

radios can cause large-amplitude spikes. The contribution of the stress cycles within each bin of the stress spectrum (Figure 9) can be evaluated using Equation 9.

$$D_j = \frac{n_j \times S_{rj}^3}{A} \tag{9}$$

where D_j is the portion of the damage accumulation ratio attributable to bin j and S_{rj} is the average stress for the cycles grouped in bin j. The data for the east and west girders are plotted in Figure 13 and provide additional evidence that the fatigue damage accumulated much more rapidly in the east girder than the west girder. The plot also provides evidence that the extremely large amplitude stress cycles (greater than 15 ksi) did not influence the accumulation of fatigue damage because the number of those cycles was so low. Stress cycles with amplitudes of approximately 7.5 ksi had the highest influence on the east girder, while stress cycles with amplitudes of approximately 6.5 ksi had the highest influence on the west girder.

The same data can be plotted in terms of the cumulative fatigue damage in order to better understand the impact of stress ranges within the stress spectrum. The cumulative fatigue data are normalized in Figure 14 by dividing the data from each girder by ΣD_j, which represents the total fatigue damage induced during the 71-day monitoring period. The differences in the rates of fatigue damage accumulation between the two girders cannot be detected from the normalized data, but approximately 95% of the fatigue damage in the east girder was induced by stress cycles between 1 and 9 ksi, while approximately 95% of the fatigue damage in the west girder was induced by stress cycles between 2 to 10 ksi. For this bridge, it did not matter if the lower bins were truncated or considered in the analysis because cycles below 1 ksi contributed less than 2.5% to the total damage. The damage at the site is dominated by typical truck traffic, whereas cycles greater than 10 ksi only contributed approximately 2.5% of the damage.

CONCLUSIONS

Using the procedures described in this paper, the amount of fatigue damage can be determined and characterized. The index stress range provides a method for assessing the relative damage accumulation between gage locations and/or bridges. Because the damage is normalized using the

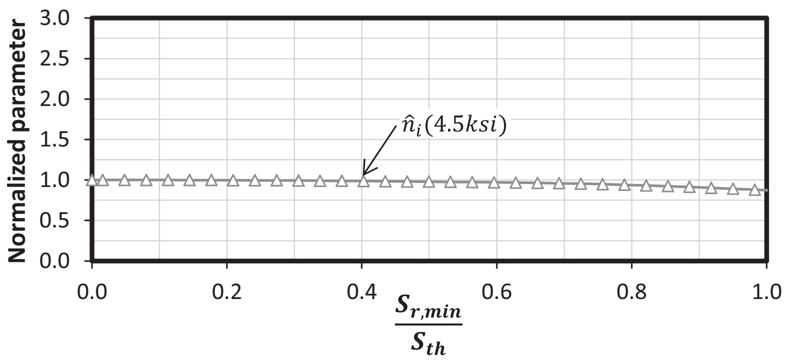

Fig. 12. Sensitivity of effective number of cycles at the index stress range to the minimum stress range retained in the stress spectrum for the east girder.

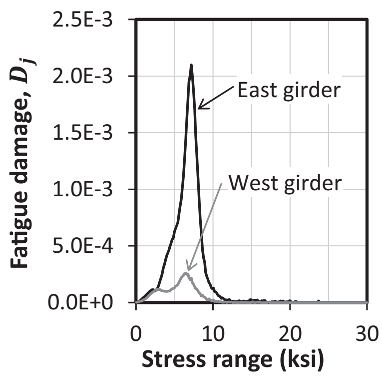

Fig. 13. Contribution of each bin to the total fatigue damage accumulated during the monitoring period.

method, the number of cycles at the index stress range is a better indicator of damage. The method can also be used to calculate the contribution of damage from each stress range. Because both low-amplitude (electromechanical noise) and high-amplitude (electomechanical spikes within the data acquisition system) stress ranges are questioned during a monitoring program, the impact of all stress ranges can be evaluated using the visualization techniques. If the cycles are contributing more to the damage than expected, those cycles can be analyzed further. Engineers can use judgment on how to handle cycles below the constant-amplitude fatigue limit, S_{th}, in the absence of international agreement. However, the lower cycles may not significantly contribute to fatigue damage (as demonstrated using the data from the fracture-critical steel bridge monitored by the research team).

ACKNOWLEDGMENTS

This research was funded by the National Institute of Standards and Technology (NIST) through the Technology Innovation Program (TIP). The opinions expressed in this paper are those of the researchers and do not necessarily represent those of the sponsor. The researchers would like to thank the bridge owner for providing access to the bridge. In addition, Vasilis Samaras, Matt Reichenbach and Ali Abu Yosef made significant contributions to the research project.

SYMBOLS

A Fatigue constant used in AASHTO (2010) design specifications to calculate fatigue life for a given detail category

D Accumulated damage ratio

D_j Portion of accumulated damage ratio corresponding to bin j of a stress spectrum

N_f Number of cycles to failure for a given constant-amplitude stress range, S_r, calculated using AASHTO (2010) design specifications

N_{fj} Number of cycles to failure for stress range S_{rj}, calculated using AASHTO (2010) design specifications

S_r Constant-amplitude stress range

S_{re} Effective stress range

$\hat{S}_{ri}$ Index stress range

S_{rj} Average stress range within bin j of a stress spectrum

$S_{r,\min}$ Minimum stress range retained in a measured stress spectrum

S_{th} Constant-amplitude fatigue limit defined in AASHTO (2010)

k Number of distinct stress ranges included within a stress spectrum

n Number of loading cycles imposed at a constant-amplitude stress range, S_r

n_j Number of loading cycles imposed at a stress range S_{rj} within a stress spectrum

$\hat{n}_i$ Effective number of loading cycles at the index stress range, $\hat{S}_{ri}$, for a given stress spectrum

n_m Total number of measured stress ranges with a stress spectrum

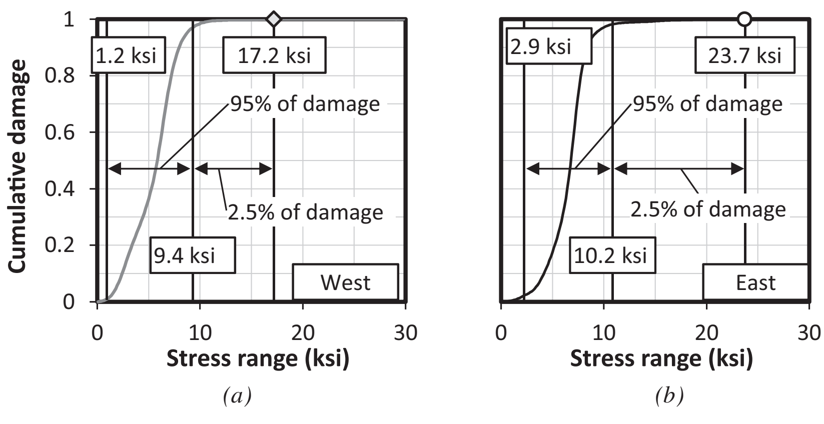

Fig. 14. Normalized cumulative damage during the monitoring period for the west (a) and east (b) girders.

REFERENCES

AASHTO (2010), AASHTO LRFD Bridge Design Specifications, American Association of State Highway and Transportation Officials, Washington, DC.

ASCE Committee on Fatigue and Fracture Reliability (1982), "Fatigue Reliabilty: Variable Amplitude Loading," *Journal of the Structural Division*, ASCE, Vol. 108, No. ST1, pp. 47–69.

ASTM (2011), Standard Practices for Cycle Counting in Fatigue Analysis, E1049-85, ASTM International, West Conshohocken, PA.

Connor, R. and Fisher, J. (2006), "Identifying Effective and Ineffective Retrofits for Distortion Fatigue Cracking in Steel Bridges Using Field Instrumentation," *Journal of Bridge Engineering,* Vol. 11, No. 6, pp. 745–752.

Dowling, N. (1972), "Fatigue Failure Predictions for Complicated Stress-Strain Histories," *Journal of Materials*, Vol. 7, No. 1, pp. 71–87.

Downing, S. and Sqocie, D. (1982), "Simple Rainflow Counting Algorithms," *International Journal of Fatigue*, Vol. 4, No. 1, pp. 31–40.

Fasl, J. (2013), "Evaluating the Remaining Fatigue Life of Steel Bridges Using Field Measurements," PhD Dissertation, The University of Texas at Austin.

Fasl, J., Helwig, T., Wood, S. L., Samaras, V., Yousef, A., Frank, K., Potter, D. and Lindenberg, R. (2010), "Development of Rapid, Reliable, and Economical Methods for Inspection and Monitoring of Highway Bridges," *Proc., IABMAS 2010*, Taylor & Francis, Philadelphia, PA.

Fasl, J., Helwig, T., Wood, S. L. and Frank, F. (2012), "Using Strain Data to Estimate the Remaining Fatigue Life of a Fracture-Critical Bridge," *Transportation Research Record*, No. 2313, pp. 63–71.

Fisher, J., Kulak, G. and Smith, I. (1998), "A Fatigue Primer for Structural Engineers," National Steel Bridge Alliance, Chicago, IL.

Li, Z., Chan, T. and Ko, K. (2001), "Fatigue Analysis and Life Prediction of Bridges with Structural Health Monitoring Data—Part I: Methodology and Strategy," *International Journal of Fatigue*, Vol. 23, pp. 45–53.

Schilling, C., Klippstein, K., Barsom, J. and Blake, G. (1978), "Fatigue of Welded Steel Bridge Members Under Variable-Amplitude Loadings," NCHRP Report 188, Transportation Research Board, Washington, DC.

Swenson, K. and Frank, K. (1984), "The Application of Cumulative Damage Fatigue Theory to Highway Bridge Fatigue Design," FHWA/TX-86/07+306-2F, Center for Transportation Research, Austin, TX.